Research Article | Vol. 26, No. 12 | 11 Jun 2018 | OPTICS EXPRESS 15705
Optics EXPRESS

# Continuous-wave and pulsed 1,066-nm Nd:$Gd_{0.69}Y_{0.3}TaO_4$ laser directly pumped by a 879-nm laser diode

**Wentao Wu,[1] Xudong Li,[1] Renpeng Yan,[1,6] Deying Chen,[1] Zhixiang Liu,[2] Xiaolin Wen,[2] Wenming Yao,[3] Fang Peng,[4] Qingli Zhang,[4] Renqin Dou,[4] and Jing Gao[3,5,7]**

[1]*National Key Laboratory of Tunable Laser Technology, Harbin Institute of Technology, Harbin 150080, China*
[2]*Shenzhen Aerospace Industry Technology Research Institute, Shenzhen 518000, China*
[3]*Jiangsu Key Laboratory of Medical Optics, Suzhou Institute of Biomedical Engineering and Technology, Chinese Academy of Sciences, Suzhou Jiangsu 215163, China*
[4]*Key Laboratory of Photonic Devices and Materials, Anhui Institute of Optics and Fine Mechanics, Chinese Academy of Sciences, Hefei 230031, China*
[5]*Tianjin Guoke Jiaye Medical Technology Development Co., Ltd, Tianjin 300399, China*
[6]*yanrenpeng@126.com*
[7]*owengaojing@126.com*

**Abstract:** We demonstrated an 879-nm-diode-pumped Nd:$Gd_{0.69}Y_{0.3}TaO_4$ laser in continuous-wave-(CW), pulse-pumped, pulse-reflection-mode *Q*-switched, and cavity-dumped burst-mode *Q*-switched operations for the first time. A maximum output power of 9.3 W at 1,066 nm was obtained in the CW operation with a slope efficiency of ~48%. The slope efficiency reached the value of ~68% in the pulse-pumped operation. A peak power of 150 kW and pulse width of 3.4 ns were obtained in the cavity-dumped burst-mode *Q*-switched operation at a *Q*-switching repetition rate of 20 kHz.



**OCIS codes:** (140.3480) Lasers, diode-pumped; (140.3380) Laser materials; (140.3530) Lasers, neodymium.

## References and links

1. F. Peng, H. Yang, Q. Zhang, J. Luo, D. Sun, W. Liu, G. Sun, R. Dou, X. Wang, and X. Xing, "Growth, thermal properties, and LD-pumped 1066 nm laser performance of $Nd^{3+}$ doped Gd/$YTaO_4$ mixed single crystal," Opt. Mater. Express **5**(11), 2536–2544 (2015).
2. Y. Ma, Z. Peng, Y. He, W. Yao, R. Yan, X. Li, X. Yu, F. Peng, Q. Zhang, R. Dou, L. Li, and J. Gao, "Continuous-wave and passively Q-switched Nd:$GYTO_4$ laser," Laser Phys. Lett. **14**(9), 095802 (2017).
3. F. Peng, W. Liu, Q. Zhang, H. Yang, C. Shi, R. Mao, D. Sun, J. Luo, and G. Sun, "Crystal growth, optical and scintillation properties of $Nd^{3+}$ doped $GdTaO_4$ single crystal," J. Cryst. Growth **406**(1), 31–35 (2014).
4. F. Peng, H. Yang, Q. Zhang, J. Luo, W. Liu, D. Sun, R. Dou, and G. Sun, "Spectroscopic properties and laser performance at 1,066 nm of a new laser crystal Nd:$GdTaO_4$," Appl. Phys. B **118**(4), 549–554 (2015).
5. W. Liu, Q. Zhang, W. Zhou, C. Gu, and S. Yin, "Growth and luminescence of M-Type $GdTaO_4$ and Tb:$GdTaO_4$ scintillation single crystals," IEEE Trans. Nucl. Sci. **57**(3), 1287–1290 (2010).
6. M. Ross, "YAG laser operation by semiconductor laser pumping," Proc. IEEE **56**(2), 196–197 (1968).
7. S. Goldring, R. Lavi, A. Tal, S. Jackel, E. Lebiush, Y. Tzuk, and E. Azoulay, "Direct pumping of four levels lasing materials," Proc. SPIE **4968**, 74–78 (2003).
8. T. Ogawa, T. Imai, K. Onodera, H. Machida, M. Higuchi, Y. Urata, and S. Wada, "Efficient pulse operation of Nd:$GdVO_4$ laser with AO Q-switch," Appl. Phys. B **81**(4), 521–524 (2005).
9. Z. Huang, Y. Huang, Y. Chen, and Z. Luo, "Theoretical study on the laser performances of $Nd^{3+}$:YAG and $Nd^{3+}$:$YVO_4$ under indirect and direct pumping," J. Opt. Soc. Am. B **22**(12), 2564–2569 (2005).
10. V. Lupei, N. Pavel, and T. Taira, "Highly efficient continuous-wave 946-nm Nd:YAG laser emission under direct 885-nm pumping," Appl. Phys. Lett. **81**(15), 2677–2679 (2002).
11. V. Lupei, N. Pavel, and T. Taira, "Efficient laser emission in concentrated Nd laser materials under pumping into the emitting level," IEEE J. Quantum Electron. **38**(3), 240–245 (2002).
12. R. Lavi, S. Jackel, Y. Tzuk, M. Winik, E. Lebiush, M. Katz, and I. Paiss, "Efficient pumping scheme for neodymium-doped materials by direct excitation of the upper lasing level," Appl. Opt. **38**(36), 7382–7385 (1999).

#323039 https://doi.org/10.1364/OE.26.015705
Journal © 2018 Received 12 Feb 2018; revised 18 May 2018; accepted 22 May 2018; published 7 Jun 2018

Optics EXPRESS

13. R. C. Stoneman, J. G. Lynn, and L. Esterowitz, "Direct upper-state pumping of the 2.8 μm $Er^{3+}$:YLF laser," IEEE J. Quantum Electron. **28**(4), 1041–1045 (1992).
14. Y. F. Ma, J. W. Zhang, H. Li, and X. Yu, "High stable electro-optical cavity-dumped Nd:YAG laser," Laser Phys. Lett. **9**(8), 561–563 (2012).
15. L. McDonagh, R. Wallenstein, and R. Knappe, "47 W, 6 ns constant pulse duration, high-repetition-rate cavity-dumped *Q*-switched $TEM_{00}$ Nd:$YVO_4$ oscillator," Opt. Lett. **31**(22), 3303–3305 (2006).
16. K. Liu, Y. Chen, F. Li, H. Xu, N. Zong, H. Yuan, L. Yuan, Y. Bo, Q. Peng, D. Cui, and Z. Xu, "High peak power 4.7 ns electro-optic cavity dumped $TEM_{00}$ 1342-nm Nd:$YVO_4$ laser," Appl. Opt. **54**(4), 717–720 (2015).
17. D. Findlay and R. A. Clay, "The measurement of internal losses in 4-level lasers," Phys. Lett. **20**(3), 277–278 (1966).

## 1. Introduction

Nd:$Gd_{0.69}Y_{0.3}TaO_4$ (abbreviated as Nd:$GdYTaO_4$ or Nd:GYTO) is a newly reported mixed laser material with a relatively short fluorescence lifetime, and broad absorption and fluorescence spectra, suitable for diode-pumped solid-state lasers with a low–to–moderate power [1,2]. Nd:$GdYTaO_4$ is a monoclinic crystal, with physical properties very similar to those of the Nd:$GdTaO_4$ crystal [3–5]. The strongest emission peak is located at ~1,066 nm under an 808-nm pumping, which corresponds to the $^4F_{3/2}\rightarrow{}^4I_{11/2}$ transition [1]. The stimulated emission cross section of the Nd:GYTO crystal at 1.06 μm is ~22 × $10^{-20}$ $cm^2$; the upper laser level $^4F_{3/2}$ has a fluorescence lifetime of ~182 μs [1,3–5]. With the broad absorption bandwidths around 809 nm and 879 nm, compared with the commonly used Nd:YAG crystal, the Nd:GYTO crystal is more favorable for the reduction of the bandwidth requirement of pumping light. Therefore, this laser crystal has the potential to improve laser efficiency. The FWHM (full width at half maximum) of the fluorescence spectrum of Nd:GYTO (~3 nm at ~1066 nm) is much wider than that of Nd:GTO (~1 nm at ~1066 nm) and Nd:YAG (<1 nm at 1064 nm). The wider fluorescence spectrum provides the potential of mode-locking uses of this crystal. Furthermore, new ultraviolet wavelength could be generated based on the 1066 nm output of the Nd:GYTO laser by utilizing the nonlinear optical conversion. The CW and pulsed solid-state lasers at infrared and ultraviolet have applications in many fields such as physical and biological researches, laser detection, laser diagnostics, laser-induced fluorescence imaging, etc.

In 2015, Peng et al. successfully grew a Nd:GYTO crystal by the Czochralski (Cz) method and demonstrated the continuous-wave-(CW) operation of the 808-nm-pumped Nd:GYTO laser for the first time. A maximum output power of 2.37 W under a pumping power of 6.5 W was obtained with a 5.2% output coupler; the slope efficiency reached 36.5% [1]. In 2017, Ma et al. demonstrated the CW and passively *Q*-switched operations of an 808-nm-pumped Nd:GYTO laser. An output power of 6.37 W with a slope efficiency of 35% were obtained in the CW operation, while an average output power of 2.26 W was obtained under a pumping power of 16.2 W in the passively *Q*-switched operation [2].

However, the Nd:GYTO crystal has a relatively low thermal performance. This crystal exhibits anisotropic thermal conductivity and anisotropic thermal diffusion coefficient. The thermal conductivities $k_a$, $k_b$, and $k_c$ of the Nd:GYTO crystal at 298 K are approximately 4.4, 3.5, and 5.2 $W\cdot m^{-1}\cdot K^{-1}$, respectively [1]. The thermal diffusion coefficients of the Nd:GYTO crystal along the *a*, *b*, and *c* axes at 298 K are approximately 1.6, 1.3, and 2.0 $mm^2\cdot s^{-1}$, respectively [1]. The thermal conductivity and thermal diffusion coefficient of the Nd:GYTO crystal are lower than those of the most commonly used laser crystals, such as Nd:YAG. The low thermal conductivity and low thermal diffusion coefficient of this crystal can lead to overheating and inhomogeneous temperature distribution during lasing. Moreover, the thermal conductivity and thermal diffusion coefficient of the Nd:GYTO crystal even decrease with the increase of the temperature. The Nd:GYTO crystal has a specific heat of approximately 29 $cal\cdot mol^{-1}\cdot K^{-1}$ at 298 K [1], which is also lower than that of the Nd:YAG crystal (approximately 39 $cal\cdot mol^{-1}\cdot K^{-1}$ at 298 K). These relatively low thermal performances can cause a harmful thermal impact in laser operations, limiting the application of the Nd:GYTO laser.

Optics EXPRESS

Direct pumping, also known as direct upper-state pumping or in-band pumping, is a pumping scheme, which directly pumps the upper laser level. This scheme was proposed for the first time by Monte Ross in 1968 [6]. The main advantages of the direct pumping over other indirect pumping schemes are the high efficiency and low waste heat [6–11]. For the $Nd^{3+}$ ion, the indirect pumping scheme at 808 nm suffers from two main drawbacks: Stokes shift and quantum efficiency losses [12]. The direct pumping reduces losses from non-radiative photon decay and bypass of the upper laser state through a self-quenching decay [13]. Therefore, the losses induced by the Stokes shift are minimized. Compared with the 808-nm pumping scheme with a theoretical quantum efficiency of 75.8%, the Nd:GYTO laser directly pumped at 879 nm has a higher theoretical quantum efficiency of 82.5%. Therefore, the waste heat can be reduced by this pumping scheme. Considering that thermal problems could hinder the development of this laser crystal owing to the relatively low thermal performance, the direct pumping scheme could be beneficial for the Nd:GYTO laser to reduce the harmful thermal effects and improve laser performances.

The electro-optical *Q*-switching technique has advantages of a high cut-off and short-pulse generation [14]. However, the gain variation could lead to a pulse-width broadening and peak-power decrease with the increase of the repetition rate. Cavity dumping is a practical approach to achieve a stable short-pulsed laser output [15, 16]. In this study, directly pumped Nd:GYTO lasers by a 879-nm laser diode (LD) in the CW, pulse-pumped, pulse-reflection-mode-(PRM) *Q*-switched, and cavity-dumped burst-mode *Q*-switched operations were demonstrated for the first time. A maximum output power of 9.3 W at 1,066 nm was obtained in the CW operation, while the slope efficiency reached ~68% in the pulse-pumped operation. A peak power of 150 kW and pulse width of 3.4 ns were obtained in the 20-kHz cavity-dumped burst-mode *Q*-switched operation.

## 2. Experimental methods

### *2.1 Experimental setups*

The *a*-cut Nd:$Gd_{0.69}Y_{0.3}TaO_4$ mixed-crystal used in our experiments had dimensions of 2 × 2 × 5 $mm^3$ and $Nd^{3+}$ concentration of 1 at.%. The thermal expansion coefficient of the Nd:GYTO crystal along the *a*-axis was smaller than those along the *b*- and *c*-axes. Therefore, the *a*-cut of the crystal helped reduce the thermal lensing effect during laser operations. The two end faces of the crystal had anti-reflective coatings at 879 nm and 1,066 nm. The crystal was wrapped with an indium foil and mounted in a copper water-cooling sink, maintained at 20 °C. An *n*LIGHT Pearl diode laser at approximately 879 nm was used as the pump source with a fiber core diameter of 400 μm and numerical aperture of 0.22.

Figure 1 shows a schematic diagram of the laser for an unmodulated CW operation and pulse-pumped operation. L1 and L2 are convex lenses ( $f_{L1} = 17.1\,\text{mm}$ , $f_{L2} = 42.8\,\text{mm}$ ), while M1 is a flat mirror with antireflection at 879 nm and high reflectivity at 1.06 μm. We employ output couplers M2 with different transmittances of 2, 5, 10, 15, 20, 25, and 30% in our experiments. L1 and L2 constitute a beam expander with a coupling ratio of 2.5, aiming to reduce the thermal effect on the crystal by expanding the focal spot (estimated to be 1.0 mm) within the crystal. The geometric cavity length of this setup is 35 mm.

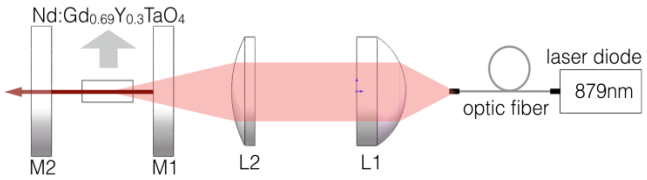


Fig. 1. Optical layout of the unmodulated Nd:GYTO laser setup.

Optics EXPRESS

Figure 2 shows a schematic diagram of the laser for the continuously pumped PRM *Q*-switched and cavity-dumped burst-mode *Q*-switched operations. L3 and L4 are convex lenses ( $f_{L3} = 34.2\,\text{mm}$ , $f_{L4} = 21.3\,\text{mm}$ ). The size of the focal spot (estimated to be 0.26 mm) is reduced to ~0.6 times of the fiber core diameter in the *Q*-switched operations to enhance the pumping rate. In the *Q*-switched operations, owing to the higher loss and longer cavity compared with those in the CW operations, a higher power density within the crystal is conducive to laser generation. As the average pumping power in the *Q*-switched operations is lower than that in the CW operations, the thermal impact caused by the focal spot size reduction is acceptable. M3 is a flat mirror with antireflection at 879 nm and high reflectivity at 1.06 μm. For the PRM *Q*-switched operation, M4 is an output coupler; for the cavity-dumped *Q*-switched operation, M4 is a flat mirror with a high reflectivity at 1.06 μm. In the figure, TFP denotes a thin film polarizer, while QWP denotes a zero-order quarter wave plate. The geometric cavity length of this setup is 190 mm.

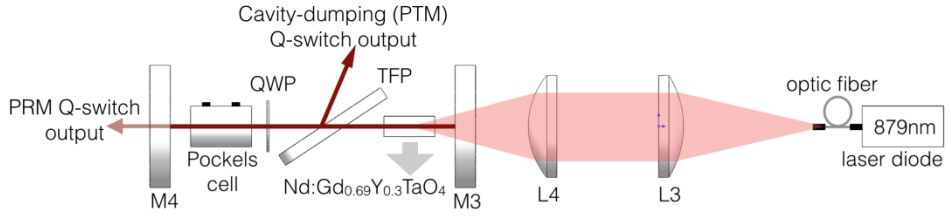


Fig. 2. Optical layout of the *Q*-switched Nd:GYTO laser setup.

The Pockels cell is made of potassium-dideuterium-phosphate (KD*P) crystals; a modulating voltage is set at the quarter-wave voltage of approximately 3,350 V. The waveforms of the driving voltage of the PRM *Q*-switched operation and cavity-dumped *Q*-switched operation are different. For the PRM *Q*-switched operation, the duration of the modulating voltage pulses is set to 900 ns. For the cavity-dumped operation, the duration of the modulating voltage pulses is set to 80 ns. The processes of the cavity-dump cycle are as follows. In step 1, no voltage is applied to the Pockels cell and lasing cannot occur. Therefore, population inversion emerges and the inverted population accumulates. In step 2, the quarter-wave voltage is applied to the Pockels cell, acting as a QWP, and lasing occurs. However, photons in the cavity cannot be output as the M4 is a reflector at 1.06 μm. In step 3, the voltage is removed, the photons in the cavity are output by the polarizer within a round-trip, and a new cycle starts. For the PRM *Q*-switched operation, as M4 is an output coupler, the lasing and output occur at the same step. Therefore, there are only two steps for one cycle.

### *2.2 Thermal simulation*

Figure 3 shows the thermal and structural simulation results of the Nd:GYTO crystal under different heat powers and pump beam diameters. The finite-element analysis software Ansys Workbench was employed to solve this model. Figures 3(a) and 3(b) show two geometric models, which simulate beams with different diameters within the crystal. In order to simulate the thermal impact, the volume of the beam within the crystal is divided into ten intervals with the same optical path length. Under certain conditions, the same heat power (one tenth of the total) is applied to each interval of the beam. In this simulation, we set the environment and cooling-water temperatures to 20 °C. The film coefficient of convection of the four side faces, in contact with the indium foil, and then with the heat sink, is set to 20 $\text{kW}\cdot\text{m}^{-2}\cdot^{\circ}\text{C}^{-1}$. The film coefficient of convection of the two end faces, in contact with air is set to 250 $\text{W}\cdot\text{m}^{-2}\cdot^{\circ}\text{C}^{-1}$.

Owing to the low thermal conductivity and cooling scheme, a relatively high temperature gradient appears in the radial direction within the crystal. This inhomogeneous temperature distribution causes thermal stress and deformation of the crystal. When a pump beam with a

Optics EXPRESS

focal spot diameter of 0.26 mm is employed (as shown in Fig. 3(a)), the highest and lowest temperatures in the crystal are ~180 °C and ~24 °C, respectively, under a heat power of 10 W. The highest temperature in the crystal decreased to ~125 °C under the same heat power of 10 W for a pump beam with a focal spot diameter of 1.0 mm (as shown in Fig. 3(b)). The maximum deformation and stress intensity decrease by ~80% and ~30%, respectively, under a heat power of 10 W for a pump beam with a larger focal spot. The same results are obtained for a pumping with a heat power of 5 W. For the same heat power, a larger focal spot diameter could reduce the maximum temperature and temperature gradient in the crystal, and consequently the thermal stress and deformation in the crystal. This result demonstrates that the crystal could utilize a larger pump energy for a wider pump beam.

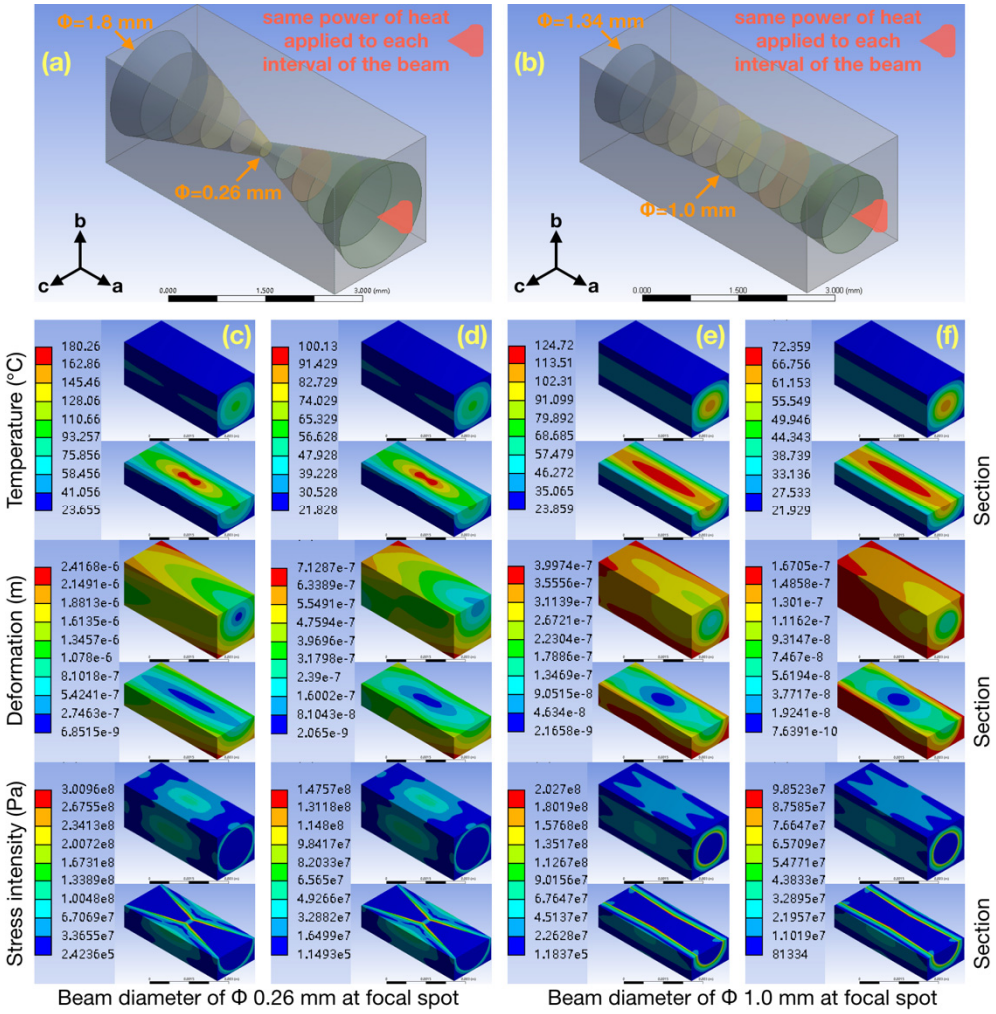


Fig. 3. Thermal and structural simulations of the Nd:GYTO crystal under different heat powers and beam diameters. Geometric models for a pumping beam with a focal spot diameter of (a) 0.26 mm and (b) 1.0 mm within the crystal. Simulation results for a (c) heat power of 10 W and focal spot diameter of 0.26 mm, (d) heat power of 5 W and focal spot diameter of 0.26 mm, (e) heat power of 10 W and focal spot diameter of 1.0 mm, and (f) heat power of 5 W and focal spot diameter of 0.26 mm.

Optics EXPRESS

## 3. Results and discussion

### 3.1 Absorption cross section at 879 nm

The absorption coefficient of Nd:GYTO at ~879 nm was investigated with a similar setup as that in Fig. 1. The LD emits a broadband amplified spontaneous emission (ASE) with a wavelength range of 860 nm to 890 nm, when it operates below the threshold current. A 2.5 × beam expander is utilized to obtain a focal spot with a diameter of ~1 mm within the crystal. The ASE spectrum is measured with and without the crystal by a fiber-coupled spectrometer (Ocean Optics HR4000, 200-1100 nm, resolution of ~0.3 nm) at room temperature; the absorption spectrum is derived from the difference.

Figure 4 shows the absorption spectrum of the Nd:GYTO crystal along the *a*-axis in the range of 870 nm to 895 nm. The absorption coefficient around 879 nm is determined to be ~2.2 $cm^{-1}$, while the full-width-at-half-maximum-(FWHM) intensity for the absorption spectrum around 879 nm is estimated to be ~1.5 nm. The absorption cross section $\sigma$ can be determined by: $\sigma = \alpha(\lambda)/N_c$, where $\alpha(\lambda)$ is the absorption coefficient, and $N_c$ is the concentration of active ions in the active medium. The concentration of $Nd^{3+}$ in the Nd:GYTO crystal is $1.67 \times 10^{20}$ $cm^{-3}$, according to an X-ray fluorescence (XRF) analysis [1]. Therefore, the absorption cross section $\sigma$ of the Nd:GYTO crystal is $1.3 \times 10^{-20}$ $cm^2$ around 879 nm.

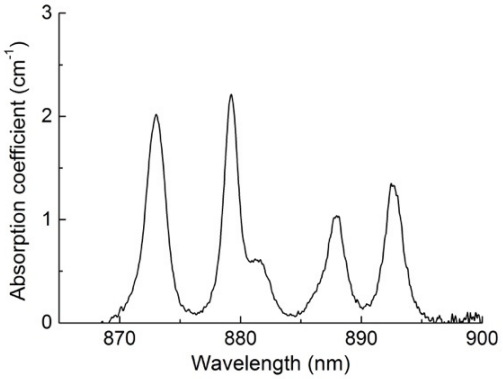


Fig. 4. Absorption spectrum of the Nd:GYTO crystal along the *a*-axis at room temperature.

### 3.2 CW operation

As shown in Fig. 5, the output power linearly increases with the absorbed pump power in the CW operation. A maximum CW output power of 9.3 W was obtained at an absorbed pump power of ~21.3 W, when the output coupler with a transmittance of 5% was employed, yielding a slope efficiency of ~48%. The output laser is linearly polarized, as measured by a Glan–Taylor prism. The Nd:GYTO crystal was damaged when the absorbed pump power reached ~22 W. The threshold absorbed pump power is approximately 1 W for all of the three output couplers. The percentages of absorption in the crystal near the threshold and at the maximum output (9.3 W) are ~70% and ~55%, respectively. The maximum output power and slope efficiency are higher than those in previous studies of the CW Nd:GYTO laser pumped at 808 nm [1,2].

Optics EXPRESS

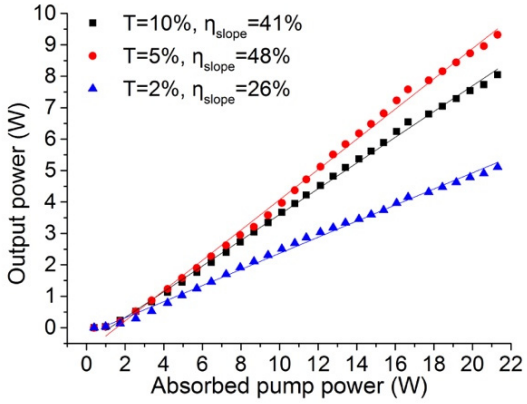


Fig. 5. Output power as a function of the absorbed power for the CW operation.

Figure 6 shows the laser intensity distribution of the Nd:GYTO laser under different pump powers in the CW operation. The laser intensity exhibits a Gaussian distribution at a low-power operation. However, as shown in Fig. 6, the laser intensity distribution deteriorates when the absorbed power increases. The deterioration of the intensity distribution at a high-power operation is mainly caused by the low thermal conductivity of the crystal. The thermal conductivities $k_a$, $k_b$, and $k_c$ of the Nd:GYTO crystal at 298 K are 4.366, 3.497, and 5.171 $W \cdot m^{-1} \cdot K^{-1}$, respectively [1], approximately 3.5 times lower than that of the Nd:YAG crystal (14 $W \cdot m^{-1} \cdot K^{-1}$). The low thermal conductivity of this crystal leads to a relatively strong thermal lensing effect and output deterioration at high-power operations.

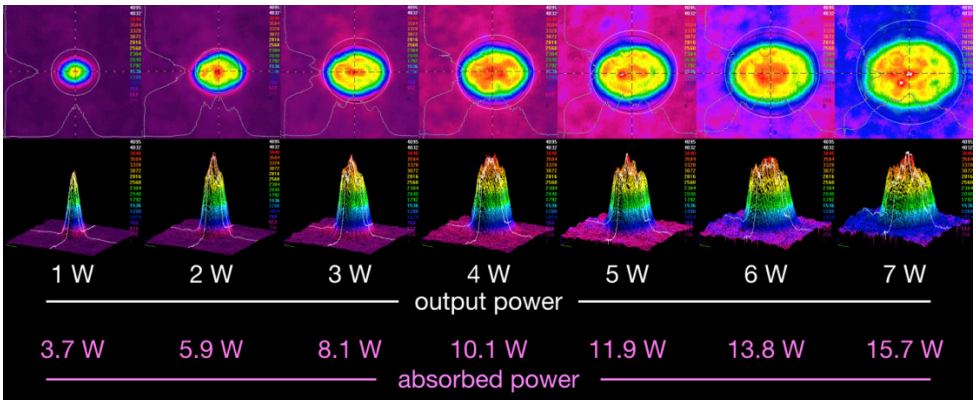


Fig. 6. Output laser intensity distributions of the CW Nd:GYTO laser under different output powers and absorbed pump powers.

The beam quality factors $M^2$, measured by a traveling 90/10 knife-edge method in two orthogonal directions, were $M_x^2 = 2.2$ and $M_y^2 = 1.4$ at an output of 1 W, $M_x^2 = 6.6$ and $M_y^2 = 4.3$ at an output of 7 W; the results are shown in Fig. 7. The beam quality deteriorates at high power operation due to the thermal lensing effect. The difference between the beam quality factors $M^2$ in the two orthogonal directions is mainly attributed to the anisotropy of the thermal conductivity of the Nd:GYTO crystal, which also leads to the oval-shaped laser intensity distributions shown in Fig. 6.

Optics EXPRESS

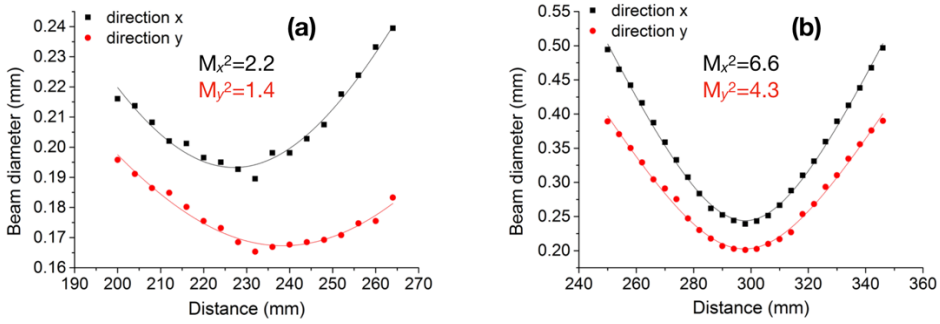


Fig. 7. Beam quality factors measured in two orthogonal directions at an (a) output power of 1 W and (b) output power of 7 W in the CW operation.

In addition, we studied the internal losses of the investigated crystal. According to the D. Findlay and R. A. Clay's study published in 1966 [17], the relationship between the threshold power and transmittance of the output coupler is determined by:

$$P_t = P_{t_0} + \frac{P_{t_0}}{2\delta L}\ln(1/R) \tag{1}$$

where $P_t$ is the threshold pump power, $P_{t_0}$ is the threshold power for a zero output coupling, $L$ is the length of the crystal, and $R$ is the reflectivity of the output coupler. The parameter $\delta$ is the total internal losses coefficient owing to absorption, scattering, and optical inhomogeneity.

We investigated the threshold pump power at output-coupler transmittances of 10, 20, 30, 40, 50, and 60%; the measured threshold absorbed pump powers at these transmittances were approximately 1.2, 1.7, 2.4, 3.2, 4.0, and 5.9 W, respectively. The data and fitting result are shown in Fig. 8.

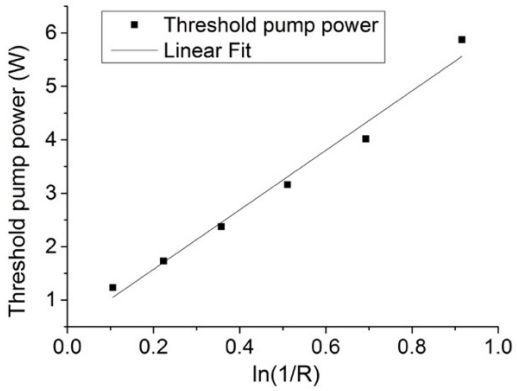


Fig. 8. Threshold pump power as a function of $\ln(1/R)$ in the CW operation.

According to the fitting result: $P_{t_0} = 0.4634$, $P_{t_0}/(2\delta L) = 5.565$. As the length of the crystal is 0.5 cm, the obtained total-internal-loss coefficient is $\delta = 0.083\ \mathrm{cm}^{-1}$.

### *3.3 Unmodulated pulse-pumped operation*

In order to reduce the thermal effect and prepare for the further burst-mode operation, we investigated the pulse-pumped operation. In this operation, the 879-nm pump laser was operated at a repetition rate of 100 Hz and pumping duration of 200 μs. The output power

Optics EXPRESS

increased linearly with the absorbed pump power in the pulse-pumped operation, as shown in Fig. 9. A maximum average output power of 0.81 W was obtained at an absorbed average pump power of ~1.4 W when the output coupler with a transmittance of 25% or 20% was used. The average value of 1.37 W (13.7 mJ per pumping duration of 200 μs) is the maximum absorbed pump power, which could be reached by our pump source in this scheme. A maximum slope efficiency of ~68% was obtained when the output coupler with a transmittance of 30% was used. Compared with the CW operation, a significantly higher efficiency was obtained as the pulsed-pumping scheme reduced the impact of the thermal effect.

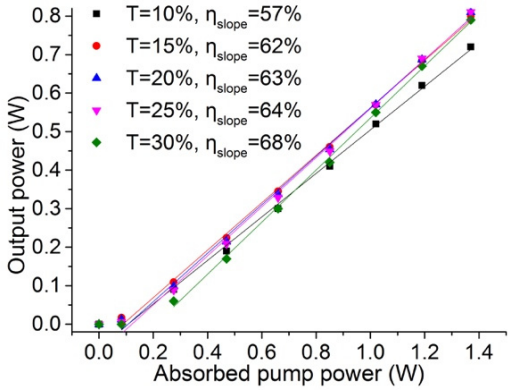


Fig. 9. Output power as a function of the absorbed power for the pulse-pumped operation.

Figure 10 shows the spectral profile of the output laser. The central wavelength was 1,066.8 nm, measured by a fiber-coupled spectrometer (Ocean Optics HR4000, 200-1100 nm) with a resolution of ~0.3 nm. During experiments in the CW and pulse-pumped operations with output couplers in the transmittance range of 2% to 30%, no changes in the wavelength were observed by the spectrometer.

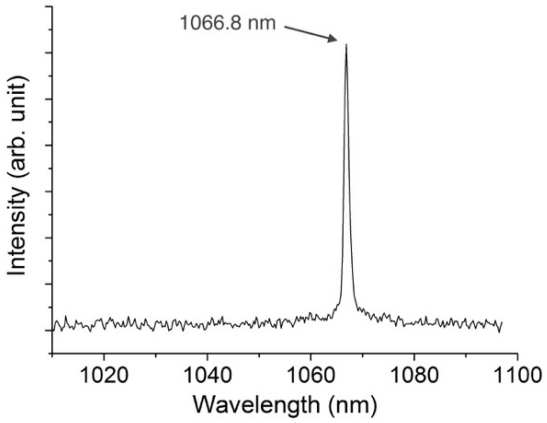


Fig. 10. Spectral profile of the output laser.

### *3.4 PRM Q-switched operation with a continuous pumping*

In the continuously pumped PRM *Q*-switched operation, we use the laser setup shown in Fig. 2. The relationships between the average output power and absorbed pump power at a *Q*-switching repetition rate of 5 kHz with different output-coupler transmittances are shown in

Optics EXPRESS

Fig. 11. A maximum slope efficiency of ~19% was obtained with an output-coupler transmittance of 15%. A maximum average output power of 0.91 W was obtained at an output-coupler transmittance of 20% and absorbed pump power of ~12.1 W.

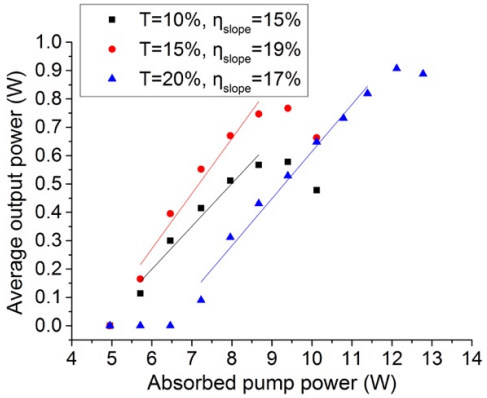


Fig. 11. Average output power as a function of the absorbed power for different output couplers.

The output power decreases when the absorbed pump power exceeds 9.4 W at output-coupler transmittances of 10% and 15%; the output power decreases when the absorbed pump power exceeds 12.1 W at an output-coupler transmittance of 20%. The origin of the decrease of the output power at a high pump power is the severe thermal impact. The low thermal conductivity of the Nd:GYTO crystal intensified the impact of the thermal effect in the continuously pumped *Q*-switched scheme. The thermal impact becomes even more severe in the operation with a lower output-coupler transmittance, owing to the increase of the intracavity laser intensity. Therefore, the optimal pump power changes with the output-coupler transmittance. The optimal transmittance of 20% for the output power is different from the optimal transmittance of 15% for the slope efficiency. However, the increase of the transmittance also causes an increase of the threshold pump power, as well as decrease of the optical–to–optical efficiency.

Figure 12 shows the relationship between the average output power and absorbed pump power with different *Q*-switching repetition rates and fixed output-coupler transmittance of 15%. A maximum slope efficiency of ~25% and maximum average output power of 0.92 W were obtained at a repetition rate of 10 kHz. In addition, the optimal pump power of 9.4 W slightly varied with the repetition rate in the range of 1 kHz to 10 kHz.

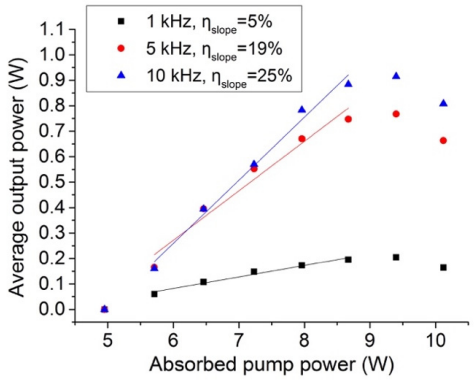


Fig. 12. Average output power as a function of the absorbed power for different *Q*-switching frequencies and fixed transmittance of the output coupler of 15%.

Optics EXPRESS

Figure 13 shows the average output power, pulse width, single pulse energy, and peak power as a function of the *Q*-switching repetition rate, for fixed absorbed power of 9.4 W and transmittance of the output coupler of 15%. At 1 kHz, the average output power, single pulse energy, peak power, and pulse width are 0.21 W, 0.21 mJ, 5.13 kW, and 40 ns, respectively, while at 10 kHz, they are 0.92 W, 0.09 mJ, 1.41 kW, and 65 ns, respectively. The pulse widened with the increase of the repetition rate.

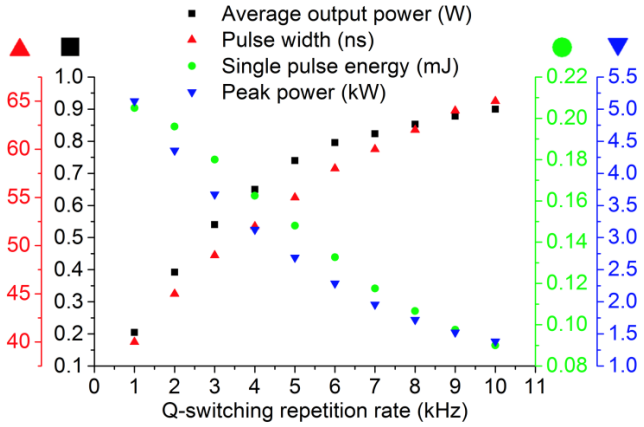


Fig. 13. Average output power, pulse width, single pulse energy, and peak power as a function of the *Q*-switching repetition rate, for fixed absorbed power of 9.4 W and transmittance of the output coupler of 15%.

### *3.5 Cavity-dumped burst-mode Q-switched operation*

For further potential applications of this laser crystal, we investigated the laser performance of the cavity-dumped operation, in order to generate short pulses with high peak power and repetition rate. In the burst-mode scheme, the 879-nm pump laser was operated at a repetition rate of 100 Hz and pumping duration of 200 μs to reduce the thermal impact. The schematic diagram of the experimental setup is shown in Fig. 2. The *Q*-switching repetition rate was set to 20 kHz. Figure 14 shows the variations of the average output power, single pulse energy, and peak power with the absorbed power. The threshold pump power is approximately 0.47 W. The output power exhibits a linear relationship with the pump power, with a slope efficiency of ~22%. The maximum slope efficiencies in the PRM *Q*-switched and cavity-dumped burst-mode operations are relatively low, compared with those in the unmodulated operations. This is mainly attributed to the higher losses introduced by the increased number of optical elements, and partially to the increased diffraction loss by the longer cavity. The average output power, single pulse energy, burst energy, and peak power were 0.21 W, 0.51 mJ, 2.1 mJ, and 150 kW, respectively, at an absorbed pump power of ~1.4 W. For operations with repetition rates over 20 kHz, loss of pulses occurs owing to the insufficient gain of the laser.

Optics EXPRESS

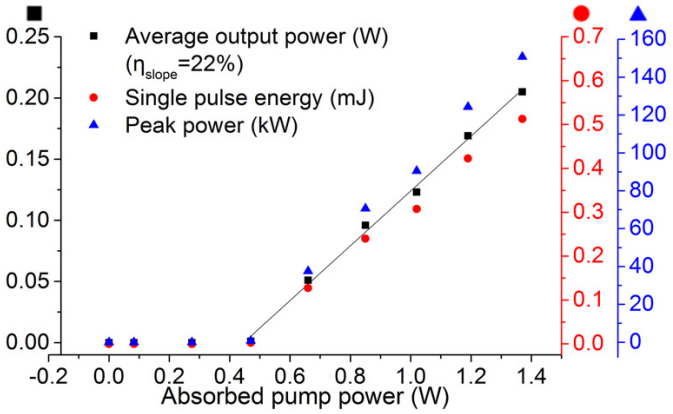


Fig. 14. Average output power, single pulse energy, and peak power as a function of the absorbed power for the cavity-dumped burst-mode *Q*-switched operation.

Figure 15 shows the output waveform profiles of the cavity-dumped burst-mode laser. The burst frequency is 100 Hz, dependent on the pumping frequency, while the burst duration is 200 μs, dependent on the pumping duration. As the *Q*-switching frequency is 20 kHz, four pulses are observed per burst. A pulse width of 3.4 ns was obtained at the 20-kHz cavity-dumped burst-mode operation, as shown in Fig. 15(c).

By employing the cavity-dumped burst-mode scheme, powerful short pulses were obtained at a high repetition rate within the burst durations. Furthermore, this high-frequency high-power short-pulsed laser can be amplified by the master-oscillator-power-amplifier-(MOPA) scheme for potential applications.

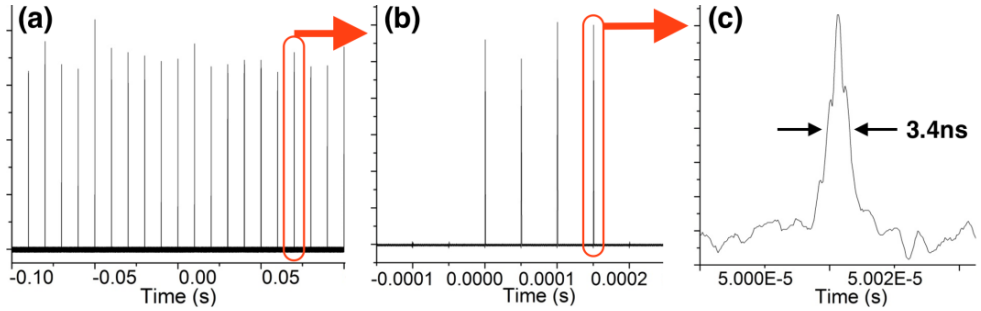


Fig. 15. Waveform profiles of the output laser for the cavity-dumped *Q*-switched operation: (a) global, (b) pulse train, and (c) single pulse.

## 4. Conclusion

In this study, 879-nm-LD-pumped Nd:$Gd_{0.69}Y_{0.3}TaO_4$ lasers in the CW, pulse-pumped, PRM *Q*-switched, and cavity-dumped burst-mode *Q*-switched operations were demonstrated for the first time. In the CW operation, the optimal output coupler, beam quality, and laser intensity distributions with different powers were investigated. A maximum output power of 9.3 W was obtained in the CW operation with a slope efficiency of ~48%. The beam quality factors $M^2$ were measured to be 2.20 and 1.35 in the two orthogonal directions at an output power of 1 W. In the pulse-pumped operation, a maximum slope efficiency of ~68% was obtained at a pumping frequency of 100 Hz and pumping duration of 200 μs. In the cavity-dumped burst-mode *Q*-switched operation, a peak power of 150 kW and pulse width of 3.4 ns were obtained at a *Q*-switching frequency of 20 kHz and pumping duration of 200 μs.

Optics EXPRESS

## Funding

National Natural Science Foundation of China (NSFC) (61605032, 61505042, 61505041); Shenzhen Science and Technology Program (JSGG20170414141239041), General Financial Grant from the China Postdoctoral Science Foundation (2015M80263, 2014M560262, 2013M531040); Special Financial Grant from the China Postdoctoral Science Foundation (2014T70336, 2015T80350); Postdoctoral Fellowship in the Heilongjiang Province (LBHZ13081, LBH-Z14074); Fundamental Research Funds for Central Universities (HIT. NSRIF. 2017018, 2015044); National Key Instrument Development Project of China (ZDYZ2013-1); Key Project of the Jiangsu Province (BE2016090, BE2016005-2); Open Fund of the State Key Laboratory on Integrated Optoelectronics (IOSKL2016KF12).